Electron Heat Transport Studies

F. Ryter[1], Y. Camenen[2], J. C. DeBoo[3], F. Imbeaux[4], P. Mantica[5], G. Regnoli[6], C. Sozzi[5], U. Stroth[7], ASDEX Upgrade, DIII-D, FTU, JET-EFDA contributors, TCV, Tore Supra and W7-AS Teams

[1] Max-Planck-Institut für Plasmaphysik, EURATOM Association, D-85748 Garching, Germany

[2] Centre de Recherches en Physiques des Plasmas, Ecole Polytechnique Fédérale de Lausanne, Association EURATOM-Confédération Suisse, CH-1015 Lausanne, Switzerland

[3] General Atomics, PO Box 85608, San Diego, California 92186-5608, USA

[4] Association Euratom - CEA, CEA/DSM/DRFC, CEA Cadarache, 13108 Saint Paul lez Durance Cedex, France

[5] Istituto di Fisica del Plasma, Associazione EURATOM-ENEA-CNR, 20133 Milano, Italy

[6] Associazione Euratom-ENEA sulla fusione, Via E. Fermi 44, 00045, Frascati, Italy

[7] Institut für Plasmaforschung, Universität Stuttgart, Pfaffenwaldring 31, 70569 Stuttgart, Germany

Abstract. Electron transport in fusion plasmas is intensively studied in coordinated experiments and great progress in physics understanding has been achieved during the last years. A threshold in normalised gradient explains most of the observations, both in steady-state and transient conditions. The results convincingly suggest that trapped electron modes dominate electron transport at low and moderate collisionality, with electron heating. The stabilisation of these modes at high collisionality predicted by theory is found in the experiments. Electron transport is then driven by the ion temperature gradient modes. At low collisionality, if trapped electron modes are stabilised by negative shear and shafranov shift effects, electron internal transport barriers may develop.

1. Introduction

In burning plasmas, the centrally peaked heating power provided by the Alpha particles will mainly be transfered to the electrons, whereas a large fraction of the ion heating will occur by electron-ion collisional transfer as energy flows towards the edge. Thus, electron heat transport is a key component for future devices. The measured electron heat transport is much larger than predicted by neoclassical theory. This is attributed to *turbulent transport* driven by micro-instabilities, which dominates transport in the electron channel. This hypothesis is supported qualitatively by fluctuation measurements, whose description is beyond the scope of this paper.
A coordinated effort and common dedicated experiments, have been conducted to understand electron transport. Several recent results suggest the existence of a threshold above which transport increases, in agreement with theoretical prediction for turbulent transport. We review here the main experimental studies on this subject covering the last 5 years. Emphasis is put on the tokamaks, but on some points a comparison with helical devices has been carried out for this work. This work deals with electron heat transport in the plasma core and does not include the edge in which the relevant physics may be quite different. Possible heat transport caused by MHD instabilities is not treated either.

2. Elements of turbulent transport theory

Theory of electrostatic turbulence indicates that electron heat transport in the plasma core may be driven by three instabilities [1, 2]: Trapped Electron Modes (TEM) [3, 4], Ion Temperature Gradient modes (ITG) and possibly Electron Temperature Gradient modes (ETG) [5]. The ITG turbulence contributes strongly to ion transport [6] and to a lesser extent to electron transport [7]. The most complete theoretical approach to characterize instabilities in the plasma core is provided by gyro-kinetic calculations, see e.g. [8]. These instabilities have respective thresholds in ion or electron normalised temperature gradients, above which turbulence and the corresponding transport increase [2]. Formulae have been derived from linear gyro-kinetic calculations for the threshold of ETG [5] and TEM [9], the former also roughly applicable to ITG by reversing the role of the species. The TEM instability being driven by trapped electrons, due to collisional detrapping, it is stabilised by increasing collisionality,

characterized by $\nu_{eff} \propto \nu_{ei}/\omega_{D_e} \approx 0.1R(Z_{eff}n_e)/T_e^2$ [10].

In the next sections, experimental results are compared with linear gyro-kinetic calculations, in particular to charaterise TEM dominated plasmas. Linear calculations do not take into account the complete physics of turbulence, but it has been shown specifically for TEM in [11] that linear and non-linear results are in good agreement, which justifies this approach.

An empirical model for electron heat transport based on the existence of a threshold $R/L_{T_e,crit}$ has been successfully tested for ASDEX Upgrade ECRH heated plasmas [12] and generalized later,[13]. It is written as:

$$\chi_e = \chi_s q^{3/2} \frac{T_e}{eB}\frac{\rho_s}{R}\left[\frac{R}{L_{T_e}} - \frac{R}{L_{T_{e,crit}}}\right]^{\alpha} H\Big(\frac{R}{L_{T_e}} - \frac{R}{L_{T_{e,crit}}}\Big) + \chi_0 \frac{T_e}{eB}\frac{\rho_s}{R} \quad (1)$$

It includes the increase of transport above the threshold $R/LT_{e,crit}$, through the Heaviside function H, as well as the gyro-Bohm factor $(T_e/eB)(\rho_s/R) \propto T_e^{3/2}$, where ρ_s is the ion Larmor radius. The dependence $q^{3/2}$ reflects the influence of the shift of the k spectrum of the modes to lower values [14], specifically investigated for the TEM in gyro-kinetic non-linear calculations [11]. It yields the required radial dependence of transport as well as its dependence with plasma current [15]. The non-dimensional coefficients χ_s, $R/L_{T_{e,crit}}$ and χ_0 are adjusted to reproduce the experimental results as well as possible. The exponent α has generally been set to unity. The increase of transport above the threshold, $\propto \chi_s q^{3/2} T_e^{3/2}$, determines the *effective stiffness* of the T_e profiles, whereas χ_s can be considered as an *intrinsic stiffness*. Consequently, plasmas with high effective stiffness, e.g. high T_e, are closer to the threshold than those with low stiffness for which R/L_{T_e} can exceed the threshold by a factor of 2 to 3 in present day tokamaks. The quantity χ_s allows for comparisons between different plasmas in various devices. We focus on the analyses carried out with this model because it has been widely used in a coherent manner in several devices.

3. Experimental approach and results in conventional scenarios

The clearest conditions to investigate electron heat transport are achieved with electron heating, at low density to reduce the coupling between electron and ion channels. The influence of sawteeth on transport and analyses must be weak, which is the case for results presented below.

The Electron Cyclotron Resonance Heating (ECRH) is the most suitable tool because its power deposition occurs only on the electrons, in a narrow layer steerable in position. For the 2^{nd} harmonic X-mode scheme, often used, the ECRH single pass absorption is generally 100%, allowing very clean experiments. In JET, for which ECRH is unfortunately not available, electron heating with ICRF in mode conversion scheme has proven useful [16]. The measurement of T_e by Electron Cyclotron Emission (ECE) heterodyne radiometers provides the required time and spatial resolutions.
Transport studies include power balance as well as investigation of transients excited by power modulation, yielding a rich set of information. The power balance analysis yields the usual electron heat diffusivity $\chi_e^{PB} = -q_e/(n_e \nabla T_e)$. The perturbative diffusivity deduced from heat pulse propagation yields $\chi_e^{HP} = -\partial q_e/\partial(n_e \nabla T_e) = \chi_e + \partial \chi_e/\partial(\nabla T_e)$. It reflects the stiffness properties, and shows that χ_e^{HP} is in general larger than χ_e^{PB}. The expression of χ_e^{HP} for the empirical model can be easily derived from Eq. 1. Experimentally, χ_e^{HP} is deduced from Fourier analysis of the T_e modulation by well-known methods [17, 18]. From amplitude and phase profiles of the perturbation one deduces respectively χ_e^{Amp} and χ_e^{phi}, yielding $\chi_e^{HP} = \sqrt{\chi_e^{Amp} \chi_e^{phi}}$.

3.1. Overview of the results and device comparisons

Numerous experiments show that the electron (and ion) temperature profiles react weakly to changes of the heating power deposition, property called profile *stiffness* or *resilience*, [19, 20, 21, 22, 23, 24, 25, 26, 27, 28]. In particular, even with strong off-axis heating, R/L_{T_e} remains clearly positive in most of the cases. A significant variation of the radial distribution of the power deposition profile is needed to vary R/L_{T_e}. This can be provided by two ECRH beams depositing their power centrally (P_{ECin}) and off-axis (P_{ECout}) and varying P_{ECin}/P_{ECout}, if possible keeping the total power constant to limit the variations of T_e. Such experiments, in L-mode, have been performed initially in ASDEX Upgrade (AUG) [15] and repeated in DIII-D [29] and TCV [30]. In AUG and DIII-D power modulation yields χ_e^{HP}. In TCV, variations of plasma triangularity (δ) indicate that electron heat transport in TEM dominated L modes decreases by about a factor of 2 from $\delta = +0.4$ to $\delta = -0.4$, [30, 31] .

The results from AUG and DIII-D agree well, Fig. 1 left plot. The three highest points for DIII-D χ_e^{HP} stand out from the trend of the others. The reason for this is not understood [29]. The power balance data clearly point toward a finite value of

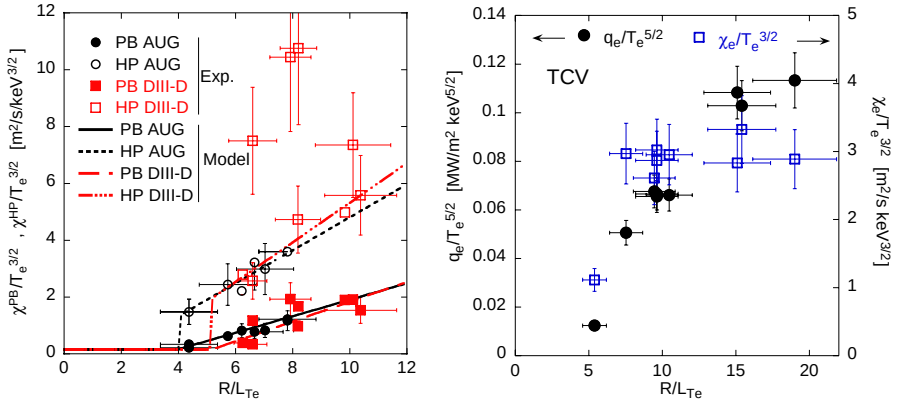

Figure 1. *Left plot: AUG and DIII-D (adapted from [29]). Normalised diffusivities versus* R/L_{T_e}*, at mid-radius. Experimental data and simulations with the empirical model for which the parameters are:* $\chi_s^{AUG} = 0.25$ $\chi_s^{DIII-D} = 0.3$, $R/L_{Te,crit}^{AUG} = 4$, $R/L_{Te,crit}^{DIII-D} = 5$.
Right plot: TCV normalised electron heat flux and diffusivity versus R/L_{T_e} *at mid-radius, for the case* $\delta = 0.2$ *(adapted from [30]).*

R/L_{T_e} for zero transport. The χ_e^{HP} and χ_e^{PB} data are compatible with the model described by Eq. 1, as shown by the lines corresponding to the parameters indicated in the caption. The differences in $R/L_{Te,crit}$ and χ_s are within the uncertainties.
In the right plot of Fig. 1 we show normalised heat flux and diffusivity versus R/L_{T_e} in TCV. Thanks to the large power density available in TCV, the range explored in R/L_{T_e}, is a factor of 2 larger than in AUG and DIII-D. Here also, χ_e unambiguously points toward a finite value of R/L_{T_e} for zero heat flux. The behaviour of q_e is almost linear which corresponds to the saturation of χ_e. This is not a transport barrier and might be attributed to an increase of the threshold linked with the increase of shear.
In ASDEX Upgrade, a comparison of the above results with linear gyro-kinetic calculations indicate that the TEM instability dominates electron heat transport [9]. The threshold and the rate of transport increase above it agree well with the experimental results. On the other hand, theory predicts the TEM-driven heat flux to be linear in R/L_{T_e} sufficiently above the threshold [9, 8]. This seems to be supported by the TCV data whereas this could not be verified in the other devices ($R/L_{T_e} < 10$) within the experimental uncertainties. It must be underlined that in these AUG and DIII-D experiments, even in the pure off-axis case, the value of

R/L_{T_e} remained most probably (just) above the threshold. Indeed, due to the low transport, the residual Ohmic heat flux was sufficient to prevent the T_e profile from dropping below the threshold. Therefore, these results strongly *suggest* the existence of a threshold in R/L_{T_e}, but could not actually *prove* its existence without ambiguity, leaving room for other interpretations [29]. Other indications of the possible existence of a threshold were reported in Tore Supra [32, 33], FTU [34, 35] and JET [16]. Results demonstrating the existence of a threshold are presented in a next sub-section.

The empirical model has also been successfully used for comparisons between devices, AUG, JET, FTU and Tore Supra, [13, 36]. The values of χ_s for dominant electron heating are in the range 0.2 - 0.5 whereas the values for the threshold cover a wide range: $3 \leq R/L_{T_{e,crit}} \leq 8$. The formula for the TEM threshold given in [9] provides a possibility to investigate the reasons of this range. The threshold given by the formula is obtained from a linear extrapolation to zero flux and the actual threshold is lower by about 70 % (see [9] figure 3). Figure 2 shows a clear relationship between the experimental threshold values and the predicted ones. The variation of $R/L_{T_e}^{TEM}$ is due to the ranges in R/L_n, $\hat{s}$ and ν_{eff} which vary significantly, as shown in the right plot of Fig. 2. These results confirm the usefulness of the empirical model and provide an experimental validation of the TEM formula.

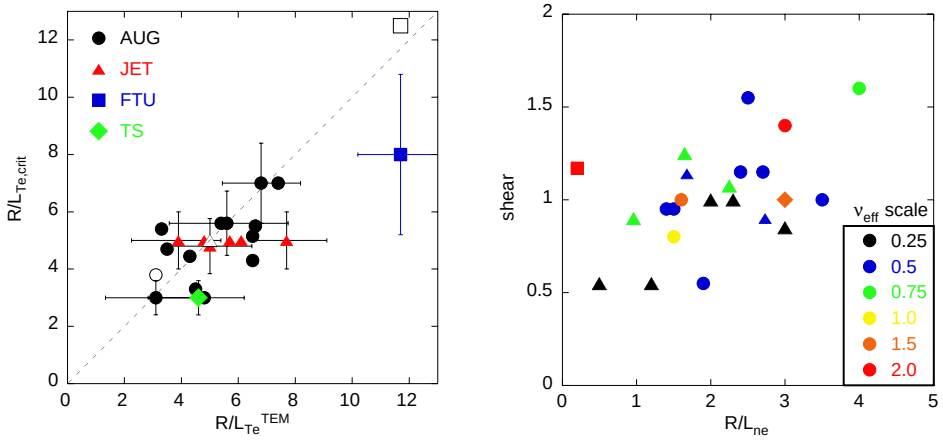

Figure 2. *Left plot: Threshold yielded by simulation with the empirical model [13] in AUG,FTU,JET and TS versus TEM threshold formula from [9] reduced by 70%. Open symbols indicate the threshold from gyro-kinetic calculations for specific discharges. Right plot: Ranges in R/L_n, $\hat{s}$ and ν_{eff} (colour code) for the same data and same symbols shape as in the left plot.*

In the results presented above with strong electron heating and $T_e > T_i$ the TEM dominate electron heat transport, the ITG contribution is small due to the low ion heat flux, TEM and ITG are not strongly coupled. In plasmas with comparable electron and ion heating, $T_e \leq T_i$, typically NBI heated L and H modes, the situation is different. The three instabilities, TEM, ITG and ETG, can coexist leading to a complicated situation. The experimental possibilities to vary R/L_{T_e} are limited, even with strong off-axis ECRH. Dedicated experiments with modulated ECRH have been carried out in DIII-D L-modes [37] and ASDEX Upgrade H-modes [38]. None of these studies provided definitive results on the type of transport. Experiments in JET with modulated ICRF could be modeled satisfactorily with the empirical model [16], the values of χ_s reaching up to about 1, [13], suggesting a possible trend for χ_s to increase with the fraction of ion heating, also found in simulations with fluid models [16].

3.2. Comparison with the W7-AS stellarator

The major electron transport issues of low-shear stellarators are neoclassical transport physics in the plasma core, with the development of the neoclassical electron root for low collisionalities [39], and the strong variation of confinement with rotational transform [40]. However, encouraged by the coherent picture in tokamaks, data from the W7-AS stellarator (shut down since 2002) have been analysed along the same line. This is justified by the gyro-Bohm dependence found in W7-AS [41], by the similarities of confinement between tokamaks and stellarators [42, 43] and by the measurement of fluctuations in the plasma core [42]. The plasmas chosen here were heated by a combination of on-axis and off-axis ECRH, see [43] figure 25 for details. In these experiments, the total heating power was varied between 0.1 MW and 0.8 MW from case to case, leading to a large variation of T_e and the gyro-Bohm normalisation is essential. The results are given in Fig. 3.

The left plot shows, here also, that the normalised heat diffusivity points toward a finite value of $R/L_{T_e} \approx 15$. Numerical simulations with the empirical model agree well with the data, as shown by the open dots in this plot and also by the T_e and χ_e profiles for two cases illustrated in the right plot. The simulations require $\chi_s = 0.2$, well within the range of ECRH heated plasmas in tokamaks. Therefore the T_e profiles are also not highly resilient and due to the relatively low temperature the effective stiffness is low. The value for the threshold is large compare to those found in tokamaks. Under

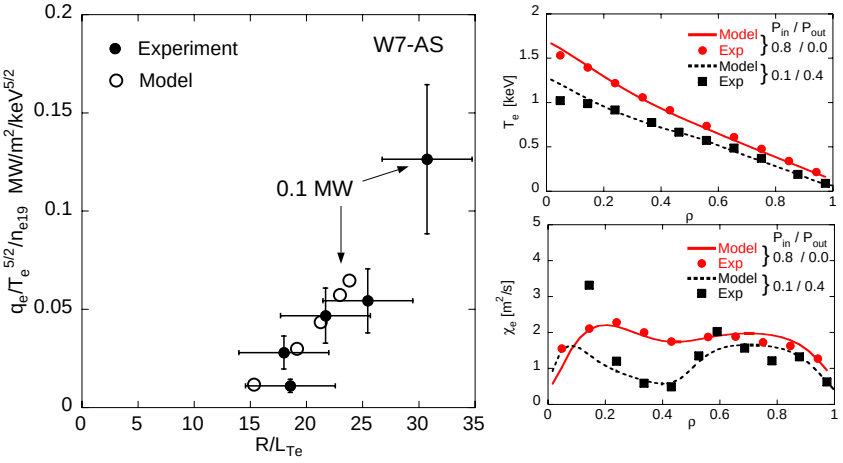

Figure 3. *Left plot: W7-AS electron heat flux versus R/L_{T_e} at mid-radius, experimental data and simulations with the empirical model. Right plot: T_e and χ_e profiles from the simulation and from experiment for 2 cases: 0.8 MW on-axis; 0.1 MW on-axis combined with 0.4 MW off-axis*

the assumption of TEM-driven transport, this may be explained qualitatively by the large aspect ratio of the device, the specific trapping configuration for electrons and by the flat shear. On the other hand, ETG modes may be active in W7-AS and a threshold formula for this device, [44], yields in this case $R/L_{T_{ETG}} \approx 13$ compatible with the experimental value. On that basis, it is not possible to conclude on the type of turbulence, but the existence of a threshold seems plausible.

The absence of Ohmic heating in stellarators makes a decisive difference for the T_e profile behaviour compared to that in tokamaks: for purely off-axis ECRH, the central heating source is rigorously zero and the T_e profiles cannot be sustained above the threshold, always leading to hollow profiles, see e.g. [45]. Therefore, this apparent contradiction between tokamaks and stellarators may be understood in the frame of the model. An argument against the hypothesis of such a type of transport has been that modulation experiments yielded $\chi_e^{HP} \approx \chi_e^{PB}$ in W7-AS, [42]. From the model, one would expect $\chi_e^{HP} \approx 3\chi_e^{PB}$. More recent data in W7-AS suggest $\chi_e^{HP}/\chi_e^{PB} > 1$ at moderate power, whereas it tends to 1 if power is further increased [46]. This might be compatible with $q_e \propto R/L_{T_e}$ discussed in [9]. The W7-AS data discussed here are only a limited subset of the database which exhibits a large variety of T_e profiles [47]. Further comparisons with the hypothesis of a threshold would be very instructive.

3.3. Experimental evidence for the R/L_{T_e} threshold

The tokamak experiments described above strongly suggest the existence of a threshold, but could not show it explicitly because the residual Ohmic power prevented the profile from dropping below the threshold. In new ASDEX Upgrade experiments at lower plasma current R/L_{T_e} could cross the threshold [48], as shown in Fig. 4.

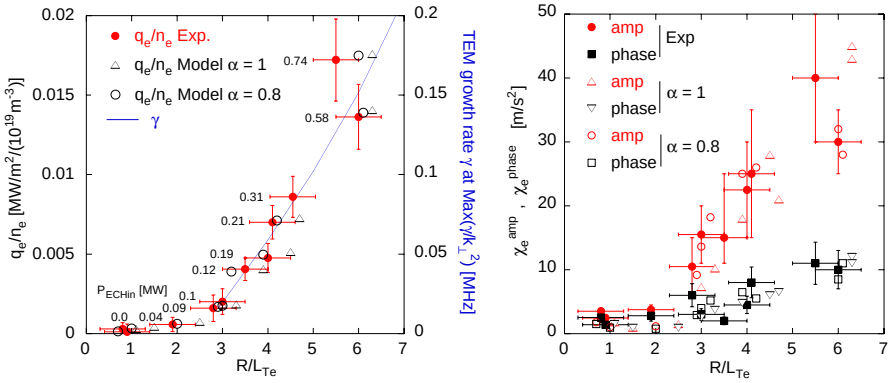

Figure 4. *Threshold in ASDEX Upgrade (from [48]). Left plot: electron heat flux versus R/L_{T_e}, experimental data and simulations with the empirical model. The line indicates the growth rate of the TEM at the maximum of $\gamma/k_\perp^2$. Right plot: χ_e^{amp} and χ_e^{phase} versus R/L_{T_e}. Experimental data and results from modeling as indicated by the legend.*

The left plot shows the dependence of the electron heat flux versus R/L_{T_e} which clearly exhibits a change of slope at $R/L_{T_e} \approx 3$, as expected for a threshold. This agrees with the linear gyro-kinetic calculations indicated by the line. The fact that q_e is low but positive below the threshold rules out the necessity of an inwardly directed heat pinch to explain the offset in R/L_{T_e}. The values of P_{ECin}, indicated for each point in the plot, show that indeed very low power (below 90 kW) is required to sustain the T_e profile just above the threshold. in the right plot the heat pulse diffusivities χ_e^{amp} and χ_e^{phi} exhibit a clear jump-like behaviour at $R/L_{T_e} \approx 3$ as expected for a threshold. Here, we find $\chi_a^{amp} > \chi_e^{phi}$ which is not usual, in general $\chi_a^{amp} \leq \chi_e^{phi}$ due to damping effects [49]. The situation found here is caused by a distortion of the amplitude and phase profiles induced by a secondary wave excited at the deposition of P_{ECin} and is considered as an additional proof for the threshold (see [48] for details).

4. Type of turbulence, transition from TEM to ITG

In ASDEX Upgrade [9], DIII-D [29], JET (done for this work) and TCV [30] gyrokinetic stability calculations indicate that with $T_e > T_i$ and for $\nu_{eff} < 1$, the TEM dominate electron heat transport. However, if collisionality is increased, the TEM are gradually stabilised and the dominant mode is found to be the ITG [48, 30]. In TCV, a decrease of transport is measured as ν_{eff} increases, Fig. 5 left plot, and the lowest normalised diffusivities are dominated by ITG, [30].

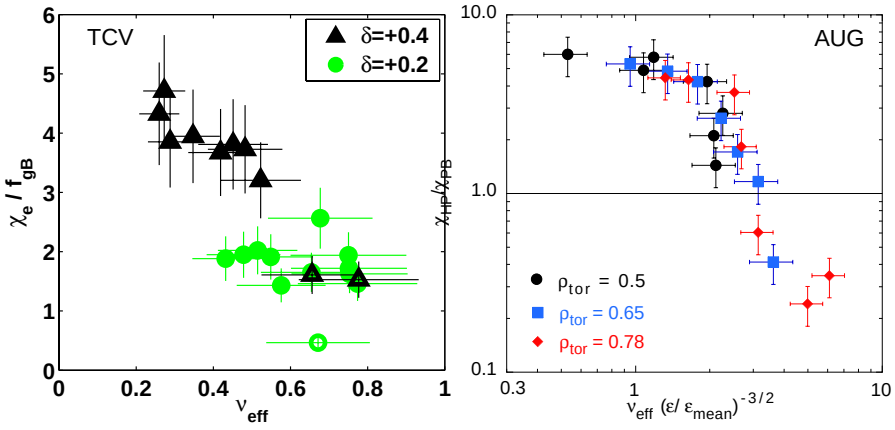

Figure 5. *Left plot TCV: Variation of normalised diffusivity versus effective collisionality (from [30]). The 3 open symbols indicate ITG dominated discharges. Right plot ASDEX Upgrade: ratio χ_e^{HP}/χ_e^{PB} versus normalised ν_{eff} (from [48]).*

In ASDEX Upgrade, modulation experiments in a collisionality scan, $0.3 < \nu_{eff} < 6$, [48], exhibit a strong drop of χ_e^{HP}/χ_e^{PB} at $\nu_{eff} \geq 2$, Fig. 5 right plot. The unusual situation $\chi_e^{HP}/\chi_e^{PB} < 1$ reflects a very weak dependence of q_e versus ∇T_e. It is interpreted as a transition from TEM to ITG dominated heat transport and explained by the different dependence versus R/L_{T_e} of the electron heat flux driven by TEM or ITG [48]. Whereas the heat flux driven by the TEM increase continuously with R/L_{T_e}, that driven by ITG saturates at $R/L_{T_e} \approx 10$ yielding very low values of χ_e^{HP}.

5. Transport in electron Internal Transport Barrier

Internal Transport Barriers characterized by large pressure gradients yield a substantial fraction of bootstrap current and high performance. Scenarios with NBI produce strong ITBs in the ion channel but generally weak or no ITBs in the electron channel [50, 51]. We focus here only on very recent results on electron ITBs created with dominant electron heating. The main studies on eITBs have been reviewed in [52] and can be found for the different tokamaks as follows: ASDEX Upgrade [53, 54]; DIII-D [55]; FTU [56, 57], JET [58, 59]; JT-60U [60, 61]; Tore Supra [62, 63]; TCV [64, 65, 66]; T-10 [67, 68] . Electrons ITBs are obtained at very low densities, with cold ions, and lead to central electron temperatures up to 20 keV. Analyses indicate that χ_e drops by almost an order of magnitude across an electron ITB, typical values inside of the barrier being 0.5 to 0.1 m^2/s [56, 58, 63, 69]. This is above the electron neoclassical value: turbulent transport is no fully suppressed. The creation of an eITB requires in general a magnetic shear profile with a local minimum, i.e. a central region with negative shear [67, 68, 59, 61, 70, 65, 66, 57]. The investigations indicate that the stabilisation of the TEM cause the eITB [71, 59, 72]. The stabilisation is found to be due to negative shear in conjunction with Shafranov shift, the latter being essential, whereas the velocity shearing plays a minor role in eITBs [71, 72].

In ASDEX Upgrade, JT60-U and TCV the strength of the barrier, for instance characterized by R/L_{T_e}, has been shown to increase with the amount of ctr-ECCD driven on the plasma axis [73, 69, 61]. In TCV, steady-state eITBs could be sustained in fully non-inductive plasmas, the current being driven by ECCD and bootstrap current [74]. Those have been used in experiments with an additional fine dosing of Ohmic current to vary the q profile which demonstrates the relation between barrier strength and negative shear [65, 66] and Fig. 6. The relationship between shear and transport in the eITB formation has been observed dynamically in Tore Supra in the so-called giant oscillations, see [75] for more details.

Attempts to diagnose eITBs using transient transport have been carried out with cold pulses in JET [76] and JT60-U [77, 78], as well as with ICRF power modulation in JET [79]. These experiments exhibit a decrease of the propagation speed of the perturbation when crossing the barrier. An example is shown in Fig. 7 for JET with modulated ICRF in the ^{3}He mode conversion scheme where the power was

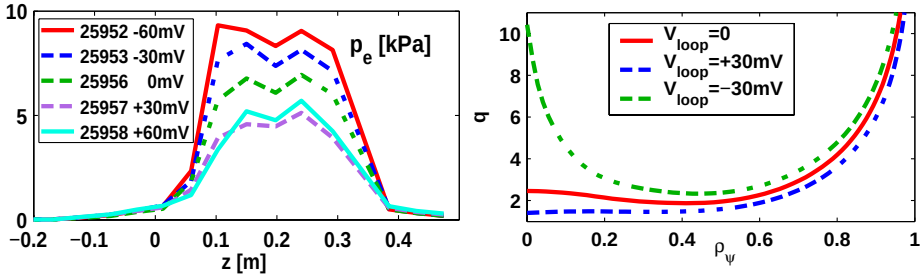

Figure 6. *Effect of q profile on eITB in TCV, (after [65]). Left plot: Electron pressure profiles for different q profiles, three of them being plotted in the right graph, identified by their corresponding loop voltage value.*

deposited at 2 positions (FW and MC). Both are modulated, complicating the heat pulse propagation pattern as the two heat waves interfere. Nevertheless, Fig. 7 indicates that in the presence of the ITB the heat waves exhibit a strong decrease of the propagation speed in the region of the barrier, as shown by the steep slope of the amplitude and phase profiles in this region, not visible in the absence of ITB.

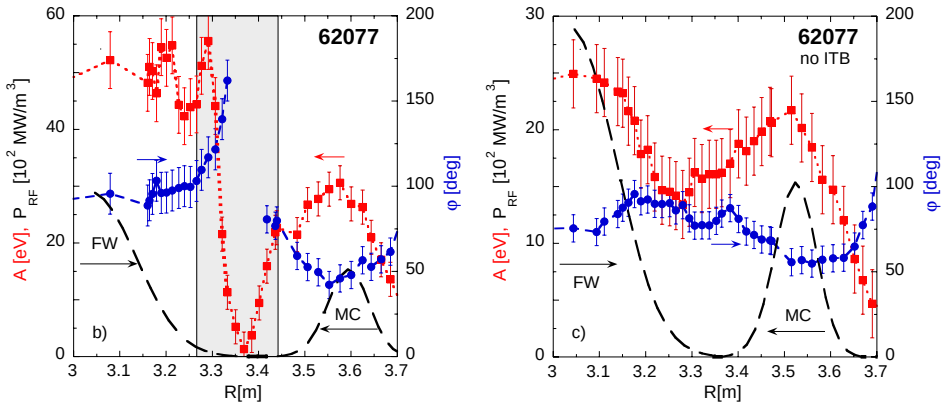

Figure 7. *Modulation data with and without ITB in JET, (after [79]). Left plot: Amplitude (red squares) and phase (blue dots) of the power modulation through an ITB in JET. Right plot: Same as left plot without ITB.*

Electron ITBs have also been investigated in helical devices as reviewed in [47] to which we refer the reader. It should be underlined that the mechanism for the eITB formation in helical devices differs from what happens in tokamaks. It is due to the transition to the electron root of transport, occurring at low collisionality and

correlated with a high positive radial electric field.

6. Conclusion

Detailed experimental studies of electron heat transport have been carried out in various devices. Power balance and heat pulse analyses yield a very complete picture of the transport properties. The experimental results in tokamaks agree with the predictions of turbulent transport theory. In the plasmas with electron heating and $T_e > T_i$ at moderate collisionality, the TEM instability is shown to dominate electron heat transport. Theory predicts a threshold which has indeed been found in the experiments. Moreover, the expected stabilisation of the TEM by collisions has also been observed, leading to a TEM-ITG transition in the electron channel. Data from the W7-AS stellarator also suggest the possible existence of a threshold.

An inwardly directed anomalous heat pinch has been often advocated to explain the resilience of T_e profiles in tokamaks. The results presented here strongly suggest that this effect is not required: a finite threshold in R/L_{T_e} and the residual Ohmic flux are found to be sufficient in most of the cases. Dedicated experiments with off-axis modulated ECRH in ASDEX Upgrade exhibit a distortion of the amplitude, which, however, is compatible with the empirical model with threshold [80]. A small heat pinch cannot be excluded to ensure $\chi_e^{PB} \geq 0$, but its values is too small to explain the distortion of the amplitude profile.

In burning plasmas, such as in ITER, electron heating will dominate and $T_e > T_i$ is expected over a significant radial region in the center of the plasma. As collisionality will be lower than in present experiments, one may expect TEM-driven transport to play a role. Further out, $T_e \approx T_i$ and the situation is complex, the different instabilities (TEM, ITG and ETG) may all be active. Its physics understanding and assessment for future devices can be achieved in present devices by further intensive studies. They should probably combine dedicated transport investigations, turbulence measurements and comparisons with non-linear gyro-kinetic calculations.

Acknowledgment

We acknowledge the support of all technical teams and colleagues in charge of

the diagnostics. The first author is grateful to C. Angioni and A.G. Peeters for their numerous explanations on transport theory. We also thank C. Bourdelle, S. Cirant, O. Sauter and F. Wagner for useful discussions and information for this paper. The work on DIII-D was partially supported by the US DOE under GA-DE-FC02-04ER54698.

References

[1] W. Horton, Rev. Mod. Phys. **3** (1999) 735.

[2] X. Garbet, Plasma Phys. Controlled Fusion **43** (2001) A251.

[3] H. Nordman et al., Nucl. Fusion **30** (1990) 983.

[4] J. Weiland, *Collective Modes in Inhomogeneous Plasmas*, IOP Publ. , Bristol, 2000.

[5] F. Jenko et al., Phys. Plasmas **8** (2001) 4096.

[6] A. Dimits et al., Phys. Plasmas **7** (2000) 969.

[7] M. A. Beer et al., Phys. Plasmas **3** (1996) 4018.

[8] F. Jenko et al., Plasma Phys. Controlled Fusion **47** (2005) B195.

[9] A. G. Peeters et al., Phys. Plasmas **12** (2005) 022505.

[10] C. Angioni et al., Phys. Plasmas **10** (2003) 3225.

[11] T. Dannert et al., Phys. Plasmas **12** (2005) 072309.

[12] F. Imbeaux et al., Plasma Phys. Controlled Fusion **43** (2001) 1503.

[13] X. Garbet et al., Plasma Phys. Controlled Fusion **46** (2004) 1351, Addendum in Plasma Physics and Controlled Fusion **47**, 6, pp. 957–958 (2005).

[14] R. E. Waltz et al., Phys. Plasmas **4** (1997) 2482 .

[15] F. Ryter et al., Nucl. Fusion **43** (2003) 1396.

[16] P. Mantica et al., 19^{th} IAEA Fusion Energy Conference, Lyon, France, Paper EX/P1-04 (2002).

[17] N. J. Lopes Cardozo, Plasma Phys. Controlled Fusion **37** (1995) 799.

[18] A. Jacchia et al., Phys. Fluids **B 3** (1991) 3033.

[19] V. Alikaev et al., Plasma Phys. Contr. Fus. Res., Proc. 11^{th} IAEA Conf., Kyoto, 1986, **3** (1987) 111.

[20] F. Wagner et al., Phys. Rev. Lett. **56** (1986) 2187.

[21] G. Taylor et al., Nucl. Fusion **29** (1989) 3.

[22] T. C. Luce et al., Phys. Rev. Lett. **68** (1992) 52.

[23] M. Greenwald et al., Nucl. Fusion **37** (1997) 793.

[24] W. Suttrop et al., Plasma Phys. Controlled Fusion **39** (1997) 2051.

[25] P. Gohil et al., Nucl. Fusion **38** (1998) 425.

[26] L. D. Horton et al., Plasma Phys. Controlled Fusion **41** (1999) B329.

[27] F. Ryter et al., Plasma Phys. Controlled Fusion **43** (2001) A323.

[28] H. Urano et al., Nucl. Fusion **42** (2002) 76 .

[29] J. C. DeBoo et al., Nucl. Fusion **45** (2005) 494.

[30] Y. Camenen et al., Plasma Phys. Controlled Fusion **47** (2005) 1971.

[31] Y. Camenen et al., 21^{st} IAEA Fusion Energy Conference, Chengdu, China (2006) EX/P3-20 .

[32] G. T. Hoang et al., Phys. Rev. Lett. **87** (2001) 125001.

[33] G. T. Hoang et al., Phys. Plasmas **10** (2003) 405.

[34] A. Jacchia et al., Nucl. Fusion **42** (2002) 1116 .

[35] S. Cirant et al., Nucl. Fusion **43** (2003) 1384 .

[36] X. Garbet et al., Plasma Phys. Controlled Fusion **46** (2004) B557.

[37] J. C. DeBoo et al., Nucl. Fusion **39** (1999) 1935.

[38] A. Manini et al., Plasma Phys. Controlled Fusion **46** (2004) 1723.

[39] H. Maassberg et al., Phys. Plasmas **7** (2000) 295.

[40] R. Brakel et al., Nucl. Fusion **42** (2002) 903.

[41] U. Stroth et al., Phys. Rev. Lett. **70** (1993) 936.

[42] H. J. Hartfuß et al., Plasma Phys. Controlled Fusion **36** (1994) B17.

[43] U. Stroth, Plasma Phys. Controlled Fusion **40** (1998) 9.

[44] F. Jenko et al., New Journal of Physics **4** (2002) 35.

[45] V. Erckmann et al., Nucl. Fusion **43** (2003) 1313.

[46] H. Walter, *Störexperimente zur Untersuchung des Energietransports im Stellarator Wendelstein 7-AS*, Doctoral thesis, Max-Planck-Institut für Plasmaphysik, Garching, Germany, 1998.

[47] F. Wagner et al., Plasma Phys. Controlled Fusion **48** (2006) A217.

[48] F. Ryter et al., Phys. Rev. Lett. **95** (2005) 085001.

[49] T. C. Luce et al., Proc. Workshop on Local Transport Studies in Fusion Plasmas (Varenna 1993), Bologna: Societa Italiana di Fisica (1994) 155.

[50] J. Connor et al., Nucl. Fusion **44** (2004) R1.

[51] X. Litaudon, Plasma Phys. Controlled Fusion **48** (2006) A1.

[52] E. Barbato, Plasma Phys. Controlled Fusion **43** (2001) A287.

[53] R. C. Wolf et al., Nucl. Fusion **41** (2001) 1259.

[54] F. Leuterer et al., Nucl. Fusion **43** (2003) 1329.

[55] C. M. Greenfield et al., in *Europhysics Conference Abstracts (CD-ROM), Proc. of the 27th EPS Conference on Controlled Fusion and Plasma Physics, Budapest, 2000*, edited by K. Szegö et al., volume 24B, pages 544–547, Geneva, 2000, EPS.

[56] V. Pericoli Ridolfini et al., Nucl. Fusion **43** (2003) 469.

[57] C. Sozzi et al., Journal of Physics: Conference Series **25** (2005) 198.

[58] G. M. D. Hogeweij et al., Plasma Phys. Controlled Fusion **44** (2002) 1155.

[59] Y. F. Baranov et al., Plasma Phys. Controlled Fusion **46** (2004) 1181.

[60] S. Ide et al., Nucl. Fusion **44** (2004) 87.

[61] T. Fujita et al., Plasma Phys. Controlled Fusion **46** (2004) A35.

[62] G. Hoang et al., Nucl. Fusion **40** (2000) 913.

[63] X. Litaudon et al., Plasma Phys. Controlled Fusion **43** (2001) 677.

[64] M. A. Henderson et al., Plasma Phys. Controlled Fusion **46** (2004) A275.

[65] O. Sauter et al., Phys. Rev. Lett. **94** (2005) 105002.

[66] T. P. Goodman et al., Plasma Phys. Controlled Fusion **47** (2005) B107.

[67] K. A. Razumova et al., Plasma Phys. Controlled Fusion **45** (2003) 1247.

[68] N. A. Kirneva et al., Plasma Phys. Controlled Fusion **47** (2005) 1787.

[69] Z. A. Pietrzyk et al., Phys. Rev. Lett. **86** (2001) 1530.

[70] M. A. Henderson et al., Phys. Rev. Lett. **93** (2004) 215001.

[71] A. G. Peeters et al., in *Proc. of the 18th IAEA Conference Fusion Energy (CD-Rom), Sorrento, Italy, October 2000*, volume IAEA-CSP-8/C, pages IAEA–CN–77/EXP5/06, Vienna, 2001, IAEA.

[72] A. Bottino et al., Plasma Phys. Controlled Fusion **48** (2006) 215.

[73] F. Leuterer et al., Nucl. Fusion **43** (2003) 744.

[74] O. Sauter et al., Phys. Rev. Lett. **84** (2000) 3322.

[75] F. Imbeaux et al., Phys. Rev. Lett. **96** (2006) 045004.

[76] P. Mantica et al., Plasma Phys. Controlled Fusion **44** (2002) 2185.

[77] S. Inagaki et al., Plasma Phys. Controlled Fusion **46** (2004) A71.

[78] S. Inagaki et al., Nucl. Fusion **46** (2006) 133.

[79] P. Mantica et al., Phys. Rev. Lett. **96** (2006) 095003.

[80] P. Mantica et al., Plasma Phys. Controlled Fusion **48** (2006) 385.